Isolation and Characterization of an Iron Biliverdin-Type Complex That Is Formed along with Verdohemochrome during the Coupled Oxidation of Iron(II) Octaethylporphyrin†,‖

Alan L. Balch,*,‡ Lechosław Latos-Grażyński,§ Bruce C. Noll,‡ Marilyn M. Olmstead,‡ and Nasser Safari‡

Contribution from the Department of Chemistry, University of California, Davis, California 95616, and Institute of Chemistry, University of Wrocław, Wrocław 50383, Poland

Received January 11, 1993®

Abstract: The coupled oxidation process, which is a model for oxidative heme degradation, has been shown to produce not only verdoheme, which was first described in 1930, but also a paramagnetic iron complex. Treatment of (OEP)-$Fe^{II}(py)_2$ (OEP is the dianion of octaethylporphyrin) with air and ascorbic acid in pyridine (py) solution yields 50% diamagnetic [(octaethyloxaporphyrin)$Fe^{II}(py)_2$]Cl, a verdoheme, and 32% paramagnetic $\{(OEB)Fe^{III}\}_2$ (OEB is the octaethylbilindione trianion, a biliverdin analog). Dimeric $\{(OEB)Fe^{III}\}_2$ has been identified by a combination of ^1H NMR and X-ray crystallographic studies. In this dimer, each iron is coordinated to four nitrogen atoms from one OEB trianion and an oxygen from another OEB ligand. Treatment of $\{(OEB)Fe^{III}\}_2$ with hydrochloric acid gives blue octaethylbilindione in 91% yield. In pyridine-d_5 solution, ^1H NMR studies show that $\{(OEB)Fe^{III}\}_2$ undergoes cleavage of the Fe–O bond to form $(OEB)Fe^{III}(py)_2$. This process is reversible.

Introduction

Heme oxygenase performs the essential role of destroying unwanted heme.[1-3] Its action is readily visible in human bruises where the conversion of purple heme to green and then yellow pigments is familiar to all readers. Scheme I shows a typical version of a widely accepted bath for the initial conversion of heme to biliverdin. Biliverdin is then converted to bilirubin by a second enzyme, biliverdin reductase. The coupled oxidation procedure, which involves air oxidation of iron(II) porphyrins in pyridine solution in the presence of a reducing agent (ascorbic acid or hydrazine), has been extensively employed as a model for the heme oxidase reaction.[4-15] This process readily produces a deep green, diamagnetic complex—verdohemochrome. Recent structural studies from this laboratory have confirmed the long-standing proposals that verdohemochrome and its derivatives

Scheme I. Heme Oxygenation[a]

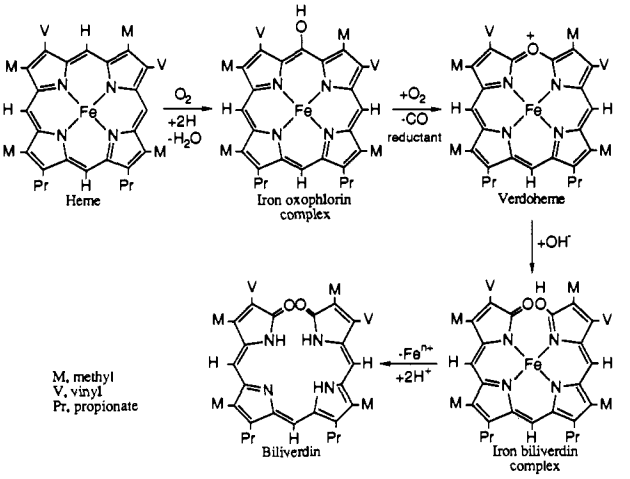

[a] Iron oxidation states and axial ligation omitted.

contain the planar, oxaporphyrin macrocycle.[16] Thus oxidation of $(OEP)Fe^{II}(py)_2$ (**1**) yields the deep green, octaethyloxaporphyrin complex $[(OEOP)Fe^{II}(py)_2]Cl$ (**2**). This is a symmetric analog of verdohemochrome. Despite the attention given to coupled oxidation over a number of years, the fact that verdohemochrome formation rarely accounts for more than 40%

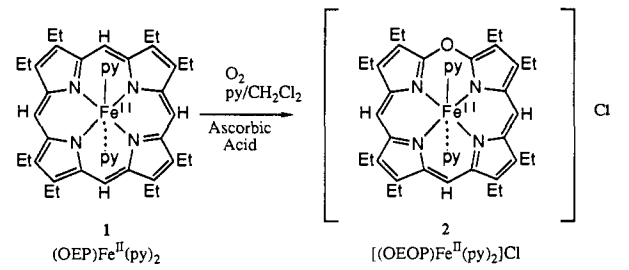

1 $(OEP)Fe^{II}(py)_2$

2 $[(OEOP)Fe^{II}(py)_2]Cl$

† Dedicated to Professor R. H. Holm on this 60th birthday.
‡ University of California, Davis.
§ University of Wrocław.
‖ Abbreviations; OEP, dianion of octaethylporphyrin; OEOP, monoanion of octaethyloxaporphrin; OEB, trianion of octaethylbilindione; py, pyridine; OEPO, trianion of octaethyloxophlorin.
® Abstract published in *Advance ACS Abstracts*, September 1, 1993.

(1) O'Carra, P. In *Porphyrins and Metalloporphyrins*; Smith, K. M., Ed.; Elsevier: New York, 1975; p 123.
(2) Schmid, R.; McDonagh, A. F. In *The Porphyrins*; Dolphin, D., Ed.; Academic Press: New York, 1979; Vol. 6, p 258.
(3) Bissell, D. M. In *Liver: Normal Function and Disease*; Ostrow, J. D., Ed.; Marcel Decker, Inc.: New York, 1986; Vol. 4, Bile Pigments and Jaundice, p 133.
(4) Warburg, O.; Negelein, E. *Chem. Ber.* **1930**, *63*, 1816.
(5) Foulkes, E. C.; Lemberg, R.; Pardonn, P. *Proc. R. Soc. London* **1951**, *B138*, 386.
(6) Lemberg, R. *Rev. Pure Appl. Chem.* **1956**, *6*, 1.
(7) Levin, E. Y. *Biochemistry* **1966**, *5*, 2845.
(8) Bonnett, R.; Dimsdale, M. J. *J. Chem. Soc., Perkin Trans. 1* **1972**, *79*, 1393.
(9) Saito, S.; Itano, H. A. *Proc. Natl. Acad. Sci. U.S.A.* **1982**, *79*, 1393.
(10) Lagarias, J. C. *Biochim. Biophys. Acta* **1982**, *717*, 12.
(11) Itano, H. A.; Hirota, T. *Tetrahedron Lett.* **1983**, *24*, 995.
(12) Sano, S.; Sano, T.; Morishima, I.; Shiro, Y.; Maeda, Y. *Proc. Natl. Acad. Sci. U.S.A.* **1986**, 531.
(13) Saito, S.; Itano, H. A. *J. Chem. Soc., Perkin Trans. 1* **1986**, 1.
(14) Masuoka, N.; Itano, H. A. *Biochemistry* **1987**, *26*, 3672.
(15) Saito, S.; Sumita, S.; Iwai, K.; Sano, H. *Bull. Chem. Soc. Jpn.* **1988**, *61*, 3539.
(16) Balch, A. L.; Latos-Grażyński, L.; Noll, B. C.; Olmstead, M. M.; Szterenberg, L.; Safari, N. *J. Am. Chem. Soc.* **1993**, *115*, 1422.

0002-7863/93/1515-9056$04.00/0

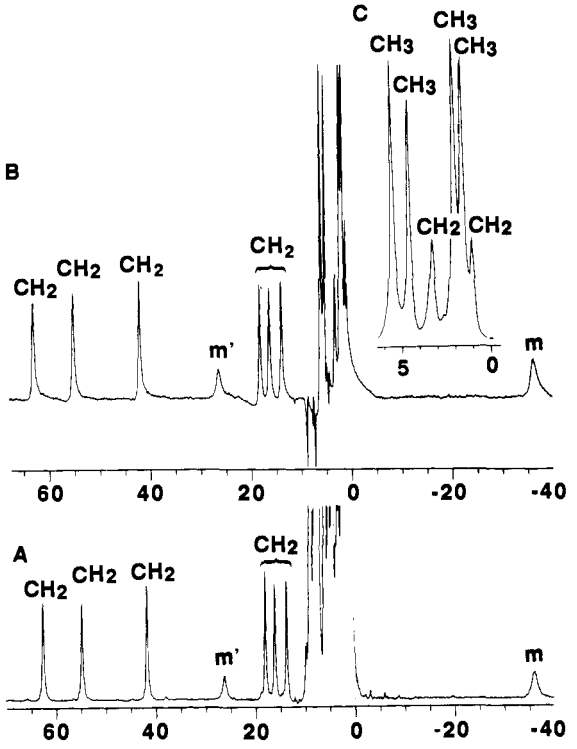

Figure 1. 300-MHz ^{1}H NMR spectra of (A) a green pyridine-d_5 solution of (OEP)Fe^{II}(py)$_2$ and ascorbic acid after addition of dioxygen, concentration by evaporation, and filtration to remove precipitated ascorbic acid at 23 °C and (B, C) a pyridine-d_5 solution of **5** at 23 °C recorded under inversion recovery conditions. Resonance assignments: m, m′, meso protons; CH_2, methylene protons; CH_3, methyl protons.

of the porphyrin employed has not been stressed. Our recent improved preparation[16] of **2** achieved a 50% yield of this green complex, but still left much material unidentified. Little attention has been given to determining where the remainder of the porphyrin goes in this process. Here we describe, for the first time, the detection and isolation of an iron complex which represents much of the missing porphyrinic material. This iron complex, which contains the biliverdin analog octaethylbilindione (**3**),[8,17] is extremely susceptible to loss of the iron ion. This sensitivity complicates characterization.

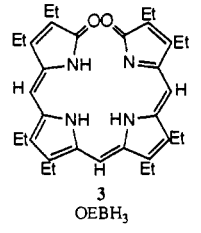

3
OEBH$_3$

Results

Addition of dioxygen to a pyridine-d_5 solution of (OEP)Fe^{II}(py)$_2$ and ascorbic acid produces a deep green solution. The electronic absorption spectrum and green color of this solution are indicative of the formation of the diamagnetic [(OEOP)Fe^{II}(py)$_2$]Cl (**2**).[10,16] The ^{1}H NMR spectrum of such a solution, after concentration and filtration to remove precipitated ascorbic acid, is shown in trace A of Figure 1. The presence of eight hyperfine shifted resonances, that are well outside of the diamagnetic envelope, clearly indicates that a paramagnetic complex is present in addition to [(OEOP)Fe^{II}(py)$_2$]Cl. The pattern of resonances seen for this paramagnetic species is different from those reported for other iron(II) and iron(III) complexes

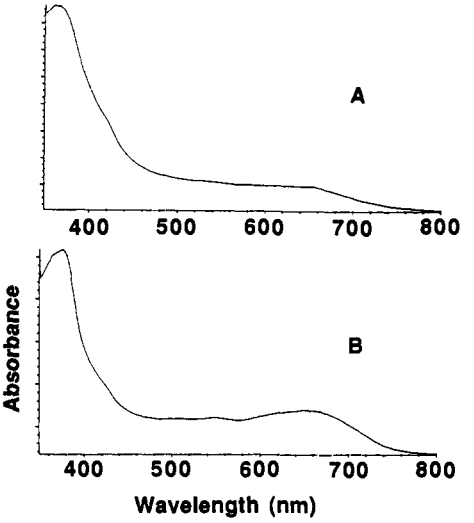

Figure 2. Electronic absorption spectra of (A) {(OEB)Fe^{III}}$_2$ (**4**) in dichloromethane solution (λ_{max}, nm (ϵ, M^{-1} cm^{-1}): 362 (6.4 × 10^4), 643 (1.6 × 10^4)) and (B) {(OEB)Fe^{III}(py)$_2$} (**5**) in pyridine solution (λ_{max}, nm (ϵ, M^{-1} cm^{-1}): 372 (3.5 ~ 104), 560 (9.4 × 10^3), 636 (9.5 × 10^3)).

of the starting porphyrin (OEPH$_2$) or to the oxaporphyrin (OEOPH).[16,18-20]

The complex that is responsible for the paramagnetically shifted component of the spectrum in Figure 1 has been separated from [(OEOP)Fe^{II}(py)$_2$]Cl and isolated. The initial separation takes advantage of the different solubilities of the two complexes in hexane. The green salt, [(OEOP)Fe^{II}(py)$_2$]Cl, is insoluble in *n*-hexane, while the dull green, paramagnetic product is soluble in *n*-hexane. Further purification of this product was accomplished by chromatography. After chromatography, the complex {(OEB)Fe^{III}}$_2$ (**4**) was obtained as a green–black solid. Characterization of this material was hampered by its air sensitivity and by the fact that it readily loses iron.

Complex **4** has also been prepared by a separate route. Treatment of the deep green [(OEOP)Fe^{II}(py)$_2$]Cl (**2**) with hydrogen peroxide in pyridine under dioxygen-free conditions produces **4** in 76% isolated yield. The spectroscopic properties (*vide infra*) of the complex prepared in this fashion are identical to those of the complex that was isolated via the coupled oxidation procedure.

Complex **4** is soluble in a range of solvents: chloroform, dichloromethane, hexane, and pyridine. Its behavior in noncoordinating solvents, particularly dichloromethane and chloroform, is similar, but in pyridine a different compound, {(OEB)Fe^{III}(py)$_2$} (**5**), is formed. The electronic spectra that are obtained from solutions of **4** in chloroform and **5** in pyridine are shown in traces A and B of Figure 2. The spectra are broad and unlike those of intact porphyrins or oxaporphyrins. However, they are similar to the spectra observed for biliverdin[21,22] and octaethylbilindione.[23]

The ^{1}H NMR spectra of **4** in chloroform and pyridine are markedly different. The spectrum obtained from chloroform solution is shown in Figure 3. The individual resonances are readily assigned on the basis of their intensities, multiplicities, and line widths. For paramagnetic iron complexes of octaethylporphyrin and core-modified derivatives such as the octaethyloxaporphyrins and octaethylazaporphyrins, the line widths

(17) Bonnett, R.; Buckley, D. G.; Hamzetash, D. *J. Chem. Soc., Perkin Trans 1* **1981**, 322.

(18) Balch, A. L.; Latos-Grażyński, L.; Noll, B. C.; Olmstead, M. M.; Zovinka, E. P. *Inorg. Chem.* **1992**, *31*, 2248.

(19) Balch, A. L.; Olmstead, M. M.; Safari, N. S. *Inorg. Chem.* **1993**, *32*, 291.

(20) Balch, A. L.; Noll, B. C.; Safari, N. S. *Inorg. Chem.* **1993**, *32*, 2901.

(21) Burke, M. J.; Pratt, D. C.; Moscowitz, A. *Biochemistry* **1972**, *11*, 4025.

(22) Chee, Q.; Song, P. S. *J. Am. Chem. Soc.* **1975**, *97*, 4176.

(23) Bonfiglio, J. V.; Bonnett, R.; Buckley, D. G.; Hamzethash, D.; Hursthouse, M. B.; Malik, K. M. A.; McDonagh, A. F.; Trotter, J. *Tetrahedron* **1983**, *39*, 1865.

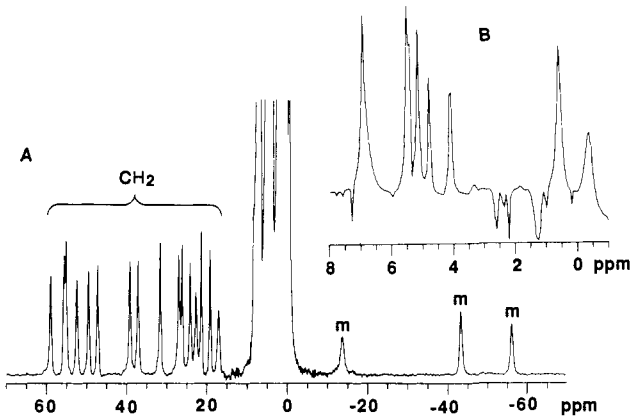

Figure 3. 300-MHz ^{1}H NMR spectrum of $\{(OEB)Fe^{III}\}_2$ (**4**) in chloroform-*d* at 23 °C. A shows the full spectrum, while inset B shows the 10 to −2-ppm region under inversion recovery conditions.

generally follow the trend of increasing line widths: methyl < methylene < meso.[16,18-20] This reflects the predominant influence of dipolar mechanisms for relaxation (where the line width is proportional to r^{-6}).[24] (Here, r is the distance between the proton and the paramagnetic center (the iron).) As a consequence of these considerations, the three broad, upfield resonances in Figure 3 have been assigned to three distinct meso protons. The 16 downfield resonances have been assigned to 16 individual methylene protons. This implies that all eight methylene groups within the ligand are in unique environments, and that each methylene group produces two resonances. Notice that there is some significant variation in the heights and line widths among these methylene resonances. In particular, the most upfield resonance has a line width that is about double that of the others. Inset B of Figure 3 shows the 10 to −2-ppm region of the spectrum taken under inversion recovery conditions. Seven resonances are clearly resolved. These can be assigned to the methyl resonances. The eighth resonance is probably not resolved. Its position cannot easily be ascertained, since under the conditions of this experiment we cannot confidently use intensity information.

Figure 4 shows a plot of the temperature dependence of the methylene and meso resonances for **4**. The plot is clearly curved for two of the meso resonances and for one of the methylene resonances. This curvature suggests that the complex may be weakly antiferromagnetically coupled.

Treatment of **4** with hydrochloric acid results in the demetalation of the complex. The free tetrapyrrole $OEBH_3$ (**3**) has been isolated from this reaction in 91% yield.

The ^{1}H NMR spectrum of $\{(OEB)Fe^{III}(py)_2\}$ (**5**) in pyridine-d_5 solution is shown in trace B of Figure 1. Remarkably, the spectrum is much simpler than that shown in Figure 3 for a chloroform solution of **4**. Using the assignment principles described above, there are only two meso resonances. The one that exhibits a downfield hyperfine shift is twice as intense as the one that has an upfield shift. There are eight distinct methylene resonances in the 50–0-ppm region. Inset C, which shows an expansion of 10 to −2-ppm region, reveals that there are four methyl resonances. It is particularly significant to note that the spectrum of **5** in pyridine corresponds to the spectrum shown in trace A of Figure 1. Thus, in pyridine, this is the species responsible for the paramagnetically shifted resonances that are produced during coupled oxidation.

The effect of temperature on the ^{1}H NMR spectrum of **5** in pyridine solution is shown in Figure 5, where the chemical shifts for the meso and methylene protons are plotted versus $1/T$ (K). Each resonance shows linear behavior. This is consistent with the presence of a monomeric complex.

(24) Swift, T. J. In *NMR of Paramagnetic Molecules*; La Mar, G. N., Horrocks, W. D., Jr., Holm, R. H., Eds.; Academic Press: New York 1973; p 53.

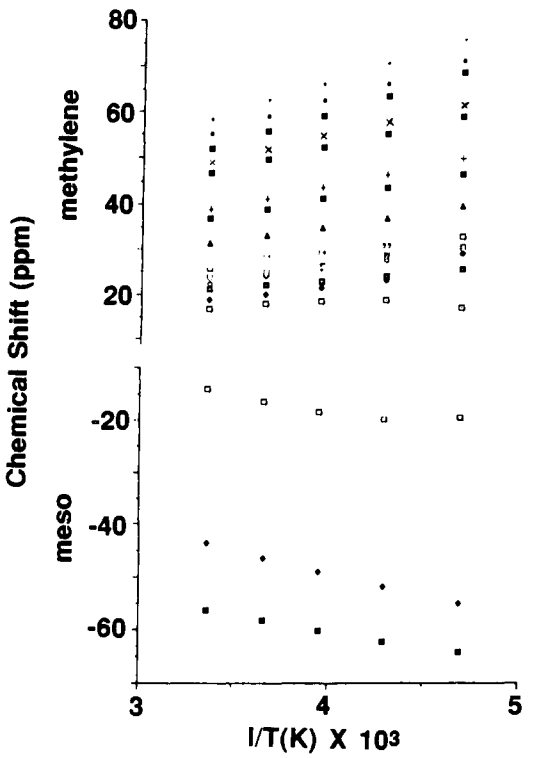

Figure 4. Plot of the chemical shift versus $1/T$ (K) for the methylene and meso resonances of **4** in chloroform-*d* solution.

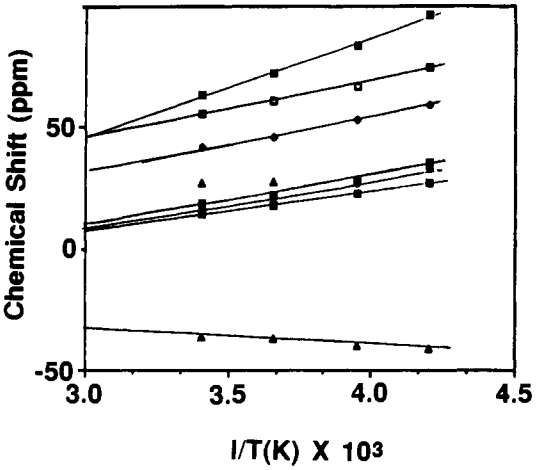

Figure 5. Plot of the chemical shift versus $1/T$ (K) for the methylene and meso resonances of **5** in pyridine-d_5 solution.

Removal of pyridine from a sample that gives the spectrum shown in trace B of Figure 1 produces a green–black solid which dissolves in chloroform to give the ^{1}H NMR spectrum shown in Figure 3. This indicates that the conversion between the two species **4** and **5** is reversible.

The EPR spectrum of **5** in frozen pyridine solution shows a strong rhombic signal at g = 6.04, 5.09, and 1.96. A second component, with a markedly different temperature dependence, consists of an axial spectrum with g = 2.10 and 1.90. These are shown in Figure 6. The relative intensities of the rhombic and axial features vary from sample to sample, and we believe that the axial component results from the presence of an impurity.

X-ray Crystallographic Analysis of $\{(OEB)Fe^{III}\}_2$ (4). The structure of **4** has been studied by X-ray diffraction. A perspective view of the complex is shown in Figure 7. Table I contains selected bond distances, and Table II reports selected bond angles.

The asymmetric unit consists of one octaethylbilindione unit and one iron ion. The iron site, however, is only partially occupied with a refined occupancy of 56(1)%. Two of these units are combined about an inversion center axis to give the dimeric

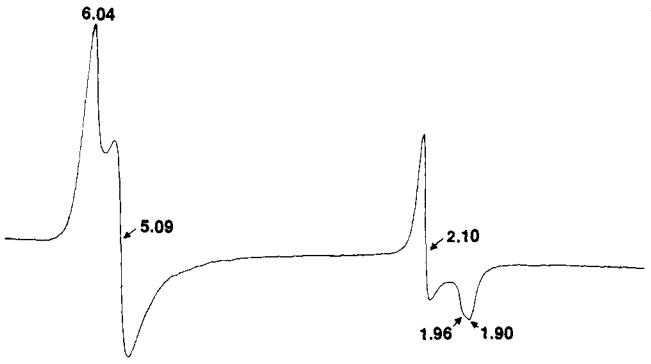

Figure 6. EPR spectrum of **5** in pyridine solution at 4.2 K.

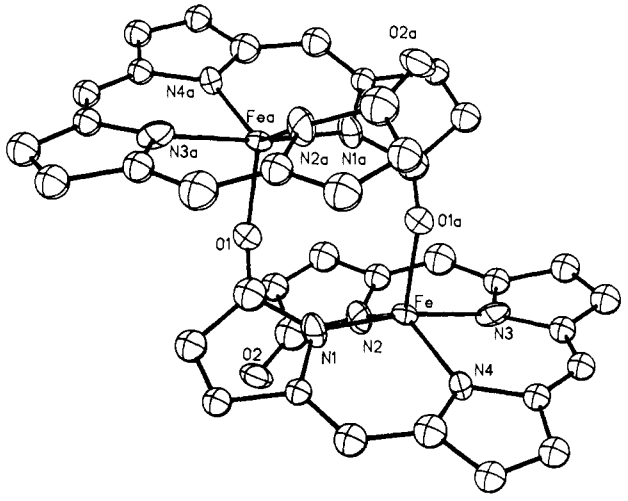

Figure 7. A perspective view of $\{(OEB)Fe^{III}\}_2$ (**4**) with 50% thermal contours for all non-hydrogen atoms. For clarity the ethyl groups have been removed.

Table I. Bond Lengths (Å) for $\{(OEB)Fe^{III}\}_2$

Fe–N(1)	2.032(12)	Fe–N(2)	2.16(2)
Fe–N(3)	2.160(13)	Fe–N(4)	2.023(15)
Fe–O(1A)	1.911(16)	O(1)–C(1)	1.32(3)
N(1)–C(1)	1.40(2)	O(2)–C(2)	1.25(3)
N(2)–C(2)	1.43(3)	N(1)–C(17)	1.34(2)
N(3)–C(7)	1.30(3)	N(2)–C(5)	1.33(3)
N(4)–C(12)	1.40(2)	N(3)–C(10)	1.43(3)
C(1)–C(19)	1.48(3)	N(4)–C(15)	1.35(2)
C(3)–C(4)	1.29(2)	C(2)–C(3)	1.51(3)
C(5)–C(6)	1.38(2)	C(4)–C(5)	1.46(3)
C(7)–C(8)	1.49(2)	C(6)–C(7)	1.47(3)
C(9)–C(10)	1.48(2)	C(8)–C(9)	1.35(3)
C(10)–C(13)	1.45(3)	C(13)–C(14)	1.32(2)
C(14)–C(15)	1.46(3)	C(16)–C(17)	1.35(2)
C(15)–C(16)	1.43(2)	C(18)–C(32)	1.42(2)
C(17)–C(18)	1.47(2)		
C(18)–C(19)	1.35(3)		

complex shown in Figure 7. Within this unit each iron ion is five-coordinate. It is bound to the four nitrogen atoms of one OEB ligand and an oxygen of the second OEB ligand. While the iron coordination is asymmetric, the angular distribution of donors about the iron ion roughly follows that of a trigonal bipyramid with the N(1)–Fe–N(3) unit as the axis. The N(1)–Fe–N(3) angle is nearly linear (171.1(7)°) and is the widest angle between any of the donor atoms. The three angles between the pseudoequatorial donors (N(2)–Fe–N(4), 135.6(7)°; N(2)–Fe–O(1A), 115.3(7)°; N(4)–Fe–O(1A), 107.6(7)°) deviate significantly from the ideal of 120° but their sum is 358.5°. Thus the group is nearly planar. The Fe–N distances show considerable variation. The two pseudoaxial Fe–N distances (2.032(12) and 2.160(12) Å to N(3)) are unequal, as are the two equatorial Fe–N distances (2.16(2) Å to N(2) and 2.023(15) Å to N(4)). For high-spin, five-coordinate (but square pyramidal) iron(III)

Table II. Bond Angles (deg) for $\{(OEB)Fe^{III}\}_2$

N(1)–Fe–N(2)	97.8(6)	N(1)–Fe–N(3)	171.1(7)
N(2)–Fe–N(3)	79.4(6)	N(1)–Fe–N(4)	90.7(6)
(2)–Fe–N(4)	135.6(7)	N(3)–Fe–N(4)	85.6(6)
N(1)–Fe–O(1A)	92.8(6)	N(2)–Fe–O(1A)	115.3(7)
N(3)–Fe–O(1A)	96.0(6)	N(4)–Fe–O(1A)	107.6(7)
C(1)–O(1)–FeA	124.8(16)	Fe–N(1)–C(1)	123.0(12)
Fe–N(1)–C(17)	124.5(10)	C(1)–N(1)–C(17)	109.3(13)
Fe–N(2)–C(2)	124.3(14)	Fe–N(2)–C(5)	121.9(16)
C(2)–N(2)–C(5)	106.5(19)	Fe–N(3)–C(7)	125.7(12)
Fe–N(3)–C(10)	123.9(13)	C(7)–N(3)–C(10)	106.6(13)
Fe–N(4)–C(12)	128.6(10)	Fe–N(4)–C(15)	123.8(11)
C(12)–N(4)–C(15)	107.4(15)	O(1)–C(1)–N(1)	125.0(15)
O(1)–C(1)–C(19)	129.8(18)	N(1)–C(1)–C(19)	104.4(17)
O(2)–C(2)–N(2)	126(2)	O(2)–C(2)–C(3)	129(2)
N(2)–C(2)–C(3)	104.5(18)	C(2)–C(3)–C(4)	109.5(19)
C(3)–C(4)–C(5)	107(2)	N(2)–C(5)–C(4)	111.7(15)
N(2)–C(5)–C(6)	123(2)	C(4)–C(5)–C(6)	124.9(19)
C(5)–C(6)–C(7)	124(2)	N(3)–C(7)–C(6)	122.8(15)
N(3)–C(7)–C(8)	112.9(18)	C(6)–C(7)–C(8)	124.2(17)
C(7)–C(8)–C(9)	104.7(16)	C(8)–C(9)–C(10)	108.4(15)
N(3)–C(10)–C(11)	122.3(13)	C(9)–C(10)–C(11)	130.5(17)
C(10)–C(11)–C(12)	128.6(17)	N(4)–C(12)–C(11)	124.4(17)
N(4)–C(12)–C(13)	106.5(12)	C(11)–C(12)–C(13)	129.0(15)
C(12)–C(13)–C(14)	109.9(16)	C(13)–C(14)–C(15)	106.4(16)
N(4)–C(15)–C(14)	109.7(13)	N(4)–C(15)–C(16)	124.4(19)
C(14)–C(15)–C(16)	125.7(17)	C(15)–C(16)–C(17)	126.8(17)
N(1)–C(17)–C(16)	123.9(13)	N(1)–C(17)–C(18)	110.5(14)
C(16)–C(17)–C(18)	125.5(15)	C(1)–C(19)–C(18)	110.1(16)

porphyrins, the range of Fe–N distances is 2.07–2.09 Å.[25,26] The Fe–O distance is 1.911(16) Å. This is slightly longer than the Fe–O distance (1.84 Å) in {(mesoporphyrin-IX DME)Fe^{III}-(OCH_3)}.[27] The C(1)–O(1) distance (1.32(3) Å) is longer than the C(2)-O(2) distance (1.25(3) Å), as expected for their respective alkoxy and keto character.

Because it is coordinated to iron, the octaethylbilindione trianion is present in a tightly coiled arrangement. This necessitates a significant distortion of the ligand from planarity in order to avoid overlap of the keto and alkoxy groups. The nonbonded separation between these oxygen atoms is 3.22 Å. The overall structure of the bilindione trianion is similar to that seen in the one other complex of this ligand that has received structural characterization.[23,28] The nickel complex of **3** has a coiled, nonplanar structure. Unlike **4**, however, it is monomeric and lacks Ni–O bonds. The two oxygen atoms lie over one another with a nonbonded separation of 3.17 Å.

Discussion

This work reveals that coupled oxidation of $(OEP)Fe^{II}(py)_2$ produces not only the verdohemochrome, $[(OEOP)Fe^{II}(py)_2]^+$, but also **4**, an iron complex of octaethylbilindione (**3**). Complex **4** is readily cleaved by pyridine to form **5**, as shown in eq 1. This reaction is reversible. Evaporation of the pyridine solution of **5** produces **4** as a green–black solid.

The coordination chemistry of biliverdin and octaethylbilindione have received very little attention.[17,23,30] As noted previously, a nickel complex of **3** has been characterized by X-ray crystallography.[23,28] It has also been reported that complexes of biliverdin-type ligands are susceptible to oxidation apparently to produce coordinated radicals.[30]

The structure of **4** is consistent with the available spectroscopic and crystallographic data. In this structure, each meso proton within one OEB unit is in a unique chemical environment (labeled

(25) Scheidt, W. R.; Reed, C. A. *Chem. Rev.* **1981**, *81*, 543.
(26) Scheidt, W. R.; Lee, Y. J. *Struct. Bonding* **1987**, *64*, 1.
(27) Hoard, J. L.; Hamor, M. J.; Hamor, T. A.; Caughey, W. S. *J. Am. Chem. Soc.* **1965**, *87*, 2312.
(28) The ambiguities in the true nature of this four-coordinate complex, which may be the nickel(II) complex Ni^{II}(OEBH), or the oxidized and deprotonated Ni^{III}(OEB) or Ni^{II}(OEB·), have been previously discussed.[23]
(29) Lewis, L. N.; Krafft, T. A.; Huffman, J. C. *Inorg. Chem.* **1992**, *31*, 3555.
(30) Subramanian, J.; Fuhrhop, J.-H.; Salek, A.; Gossauer, A. *J. Magn. Reson.* **1974**, *15*, 19.

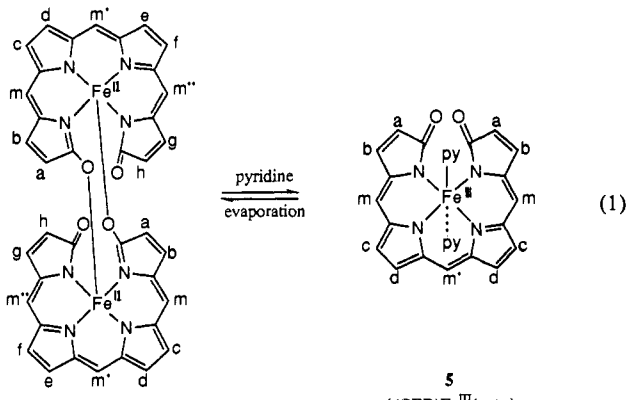

(1)

4
a-h = ethyl
m, m', m'' = H

5
{(OEB)Fe^{III}(py)$_2$}
a,b,c,d = ethyl
m, m' = H

m, m′, and m″), but the two OEB moieties themselves are equivalent. Also each ethyl group within one OEB trianion is in a chemically distinct environment (labeled a–h). Moreover, there is no symmetry element that renders the two methylene protons of each of these ethyl groups equivalent. Consequently the ^{1}H NMR spectrum of **4** in chloroform displays 16 distinct methylene resonances. The noticeable variation in the line widths of the methylene and meso resonances in Figure 3 is readily explained by the dimeric nature of the complex. The presence of two paramagnetic centers within the molecule places some groups of each class (meso, methylene) closer to the iron ion in the adjacent OEB moiety. This causes additional broadening of the resonances of those groups. Similar differential line width variations have been observed and thoroughly analyzed in the related oxophlorin dimer {(OEPO)Fe^{III}}$_2$.[18] The curvature seen in the Curie plot (Figure 4) for **4** and our inability to detect an EPR spectrum for this complex suggest that there is a weak antiferromagnetic coupling between the two iron(III) ions. Similar features have been observed for the related dimer {(OEPO)Fe^{III}}$_2$.[18]

The interpretation of the crystallography for **4** is complicated by the observation of only partial occupancy of the iron site. Such partial occupancy is unusual but not unprecedented. For example, the crystal structure of Pt_2(dibenzylideneacetone)$_3$ shows the presence of two platinum sites. One is fully occupied, while the other has 44% occupancy.[29] We proposed that the crystals that we have studied are made up of a disordered mixture of molecules of **4** and a second compound **6**, in which one of the iron ions has

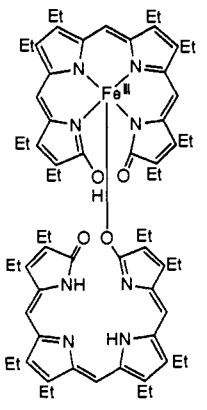

6

been replaced by protons. Despite repeated efforts that have utilized a variety of crystallization conditions, we have not been able to obtain better quality crystals of **4**. It is important to note that the observation of partial occupancy of the iron site is entirely consistent with the chemical properties of the complex. We have shown that **4** can be purposely demetalated by acid to form **3**, and we have also observed that **4** is readily demetalated during routine chemical handling. The medium used for crystallization of **4** employed acetonitrile, a solvent with reasonable ability to solvate the iron ions that would be formed during demetalation. This may have facilitated the loss of iron during the slow crystallization process. This may have facilitated the loss of iron during the slow crystallization process.

Dissolution of **4** in pyridine results in its conversion into a new species, {(OEB)Fe^{III}(py)$_2$} (**5**). On removal of pyridine, this complex loses the axial pyridine ligands and reverts back to {(OEB)Fe^{III}}$_2$ (eq 1). A similar relationship between a dimeric and monomeric structure is seen in oxophlorin complexes (eq 2,

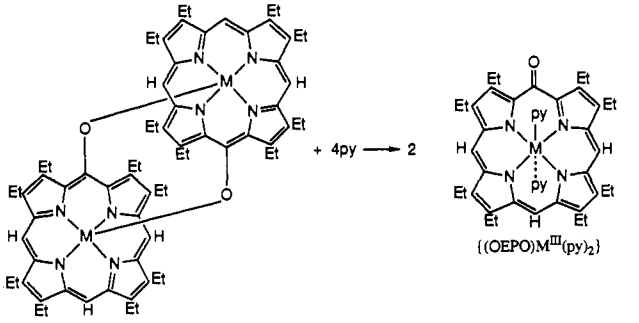

(2)

M = Fe, Mn).[14,18,31,32] In cases with both OEB and OEPO as ligands, the dimer-to-monomer transformation is accompanied by breaking of the pseudoaxial M–O bonds that serve to hold the dimers together.

The structure we propose for **5** is supported by the spectroscopic data, especially the ^{1}H NMR data. This structure is viewed as having a C_2 axis that passes through Fe and the meso group m′. We visualize the resulting molecule as similar to what would be produced if two axial pyridine ligands were added to the structure of the nickel complex of **3**.[23,28] In such a molecule, there are two types of meso protons and four types of ethyl groups. This explains the presence of only two meso and four methyl resonances in the spectrum shown in trace B of Figure 1. Each methylene group, however, is diastereotopic, and there are eight distinct methylene protons and eight methylene resonances for **5**. The EPR spectrum of **5** is consistent with the presence of high-spin ($S = {}^5/_2$) Fe(III) in the low-symmetry environment that this structure provides. As a reviewer pointed out, it is also possible that the pyridine solutions of **4** contain the five-coordinate {(OEB)Fe^{III}(py)}. In that case, in order to explain the symmetry that the ^{1}H NMR spectra require, there would have to be rapid exchange of coordinated pyridine on either side of the OEB ligand.

Previous work has shown that the reaction between iron(III) and biliverdin can produce verdohemochrome.[13] That is, ring closure of the open chain tetrapyrrole can occur upon metalation. Also it has been shown that verdohemochrome is converted to free biliverdin in 2-picoline upon treatment with (a) ascorbate/O_2, (b) hydrogen peroxide/phenylhydrazine, or (c) aqueous potassium hydroxide.[9] These reactions are, however, not observed in pyridine solution. The present study has shown that the verdoheme analog **2** is converted into **4** through treatment with hydrogen peroxide. This conversion involves both oxidation of iron and hydrolysis of the oxaporphyrin in **2**. Although the stoichiometric reaction shown in eq 3 can be written for this transformation, we have only qualitatively shown that the conversion does occur but have not verified that the stoichiometry of eq 3 holds. Although reaction 3 may account for the formation of **4** in the coupled oxidation process, further study is required to determine whether **2** and **4** are formed by parallel or sequential routes. So far we have not found evidence that either **4** or **5** is

(31) Morishima, I.; Shiro, Y.; Wakino, T. *J. Am. Chem. Soc.* **1985**, *107*, 1063.
(32) Balch, A. L.; Noll, B. C.; Reid, S. M.; Zovinka, E. P. *Inorg. Chem.* **1993**, *32*, 2610.

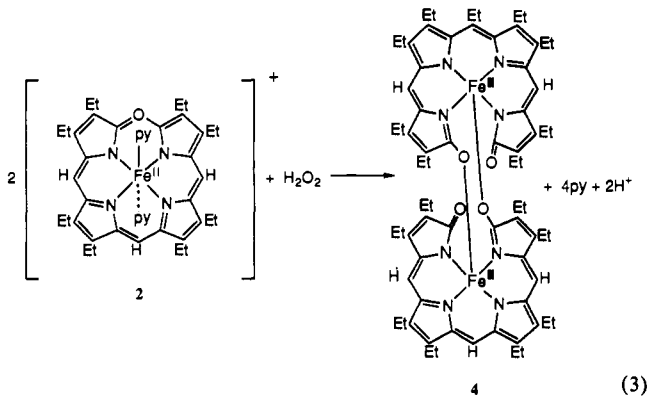

(3)

readily converted back to **2**. In particular, in pyridine solution, **5** appears to be sufficiently stable so that it does not undergo reduction and ring closure to form **2**.

In summary, we have identified that a significant portion of the missing material in the coupled oxidation process is a paramagnetic iron complex of octaethylbilindione (**3**). In pyridine solution, this is present as the monomer $\{(OEB)Fe^{III}(py)_2\}$ (**5**), but upon removal of pyridine, **5** is converted to the dimer $\{(OEB)Fe^{III}\}_2$ (**4**). Further examination of the role of these compounds in the coupled oxidation process are in progress, as are studies designed to identify the approximately 18% of the product that is still not characterized.

Experimental Section

Preparation of Compounds. $\{(OEB)Fe^{III}\}_2$ (4). 4 was obtained by a variation on standard routes of verdohemochrome formation.[10,16] A 500-mg sample of ascorbic acid was added to a solution of 100 mg of (OEP)-$Fe^{II}(py)_2$ in 6 mL of pyridine. A 50-mL portion of dichloromethane which was saturated with dioxygen was added. The mixture was shaken for 5 min. The green solution was filtered to remove any insoluble material, and the filtrate was washed with two 50-mL portions of water. The resulting green solution was dried by passage through a 5-cm-thick layer of anhydrous sodium sulfate. The sample was reduced under vacuum until a green precipitate formed. At this stage, an additional 10-mL portion of *n*-hexane was added. The deep green precipitate was collected by filtration and washed with *n*-hexane to remove a dark blue-green substance (yield: 52 mg, 50%). This solid is the verdohemochrome analog $[(OEOP)Fe^{II}(py)_2]Cl$, which has been characterized previously.[10,16]

The solution and *n*-hexane washings that remained after the isolation of the verdohemochrome were combined and evaporated to dryness at room temperature. The dark solid that remained was dissolved in dichloromethane (4 mL) and subjected to chromatography on 4 × 2 cm silica gel column under dioxygen-free conditions. Elution of the column with dichloromethane produced a reddish band which was set aside. Further elution with a dichloromethane/methanol (100:3; v/v) mixture produced a dull green band which was collected and evaporated to dryness to give **4** (yield: 26 mg, 32%). Anal. Calcd. for $C_{70}H_{84}Fe_2N_8O_4 \cdot 0.26CH_2Cl_2$: C, 68.20; H, 7.05; N, 9.06; Cl, 1.49. Found: C, 67.05; H, 7.16; N, 9.43; Cl, 1.47. The presence of dichloromethane was verified in the ^1H NMR spectrum. The UV/vis spectrum is reported in Figure 2, and the ^1H NMR spectrum in chloroform-*d* solution is presented in Figure 3.

Isolation of $OEBH_3$ from $\{(OEB)Fe^{III}\}_2$. Under a dinitrogen atmosphere, 2 mL of 1 M aqueous hydrochloric acid was added to a green solution of 18 mg (0.015 mmol) of $\{(OEB)Fe^{III}\}_2$ in 15 mL of acetone. The resulting blue solution was allowed to stand for 2 h, and then it was poured into 30 mL of ice water. The mixture was extracted with three 10-mL portions of dichloromethane. These were combined, dried over a solid sodium sulfate, and then filtered to remove the desiccant. The solution was evaporated to dryness to yield 15 mg (0.027 mmol, 91%) of blue $OEBH_3$. This was identified by comparison of its electronic absorption and ^1H NMR spectra with those of an authentic sample.[8,21]

Conversion of $\{(OEOP)Fe^{II}(py)_2\}Cl$ (2) to $\{(OEB)Fe^{III}\}_2$ (4). A 50-mg (0.064 mmol) sample of $[(OEOP)Fe^{II}(py)_2]Cl$ in 15 mL of dioxygen-free pyridine was slowly treated with 20 μL (0.02 mmol) of 30% hydrogen peroxide which had been flushed with dinitrogen. Within 5 min the color of this mixture changed from deep green to dull green. The solvent was removed by vacuum evaporation at 40 °C. The solid was dried under vacuum for 18 h and then purified by chromatography. The 2-cm-diameter column was packed with 1 cm of sodium sulfate, 4 cm of silica gel, and 2 cm of sodium sulfate. The sample was dissolved in a minimum of dichloromethane and applied to the column. Elution utilized a 100:2 v/v mixture of dichloromethane and methanol. The dull green band was collected and evaporated to dryness to give 30 mg (78%) of $\{(OEB)-Fe^{III}\}_2$, which was identified by its spectroscopic characteristics.

Table III. Crystal Data and Data Collection Parameters for $\{(OEB)Fe^{III}\}_2$

formula	$C_{35}H_{42}Fe_{0.56}N_4O_2$
fw	581.8
color and habit	dark red block
crystal system	triclinic
space group	$P\bar{1}$
a, Å	10.040(3)
b, Å	12.011(4)
c, Å	14.134(4)
α, deg	111.18(2)
β, deg	95.19(3)
γ, deg	102.24(2)
V, Å^3	1526.8(8)
T, K	123
Z	2
cryst dimens, mm	0.12 × 0.08 × 0.06
d_{calcd}, g cm^{-3}	1.266
radiation (λ, Å)	Cu Kα, (1.541 78)
μ, mm^{-1}	2.627
range of transm factors	0.80–0.88
no. of data collected	3643
no. of unique data	3632
no. of data used in refinement	1220 ($F > 6\sigma(F)$)
no. of parameters refined	205
R^a	0.115
$R_w{}^a$	0.123

^{a} $R = \sum||F_o| - |F_c||/|F_o|$ and $R_w = \sum||F_o| - |F_c|w^{1/2}/\sum|F_o|w^{1/2}$; $w^{-1} = \sigma^2(F) + 0.0296F^2$

X-ray Data Collection. Suitable, but small, crystals from **4** were obtained by diffusion of acetonitrile into a dichloromethane solution of the complex. A crystal was coated with a light hydrocarbon oil and mounted in the 123 K dinitrogen stream of a Siemens P4/RA diffractometer equipped with a locally modified LT-2 low-temperature apparatus. Intensity data were collected using Ni-filtered Cu Kα radiation from a Siemens rotating anode operating at 15 kW. Crystal data are given in Table III. Two check reflections showed only random (<2%) variation in intensity during data collection. The data were corrected for Lorentz and polarization effects. Further details are given in the supplementary material.

Solution and Structure Refinement. Calculations were performed on a DEC VAX station 3200 with SHELXTL Plus v. 4.2. Scattering factors and correction for anomalous dispersion were taken from a standard source.[33] An absorption correction was applied.[34] The solution was determined from the Patterson map and subsequent cycles of least-squares refinement and calculation of difference Fourier maps.

Instrumentation. ^1H NMR spectra were recorded on a General Electric QE-300 FT NMR spectrometer operating in the quadrature mode (^1H frequency is 300 MHz). The spectra were collected over a 50-KHz band width with 16 K data points and a 5-μs 45° pulse. For a typical spectrum, between 1000 and 5000 transients were accumulated with a 50-ms delay time. The signal to noise ratio was improved by apodization of the free inducing decay. Electronic spectra were obtained using a Hewlett Packard diode array spectrometer. EPR spectra were obtained with a Brucker spectrometer that operates at *x*-band.

Acknowledgment. We thank NIH (GM-26226) for financial support.

Supplementary Material Available: Tables of crystal data, data collection, and a structure solution and refinement summary as well as atomic positional parameters, bond distances, bond angles, and anisotropic thermal parameters and two drawings of $\{(OEB)-Fe^{III}\}_2$ (10 pages); listings of observed and calculated structure factors (5 pages). Ordering information is given on any current masthead page.

(33) *International Tables for X-ray Crystallography*; Kynoch Press: Birmingham, England, 1974; Vol. 4.

(34) The method obtains an empirical absorption tensor from an expression relating F_o and F_c. Moezzi, B. Ph.D. Thesis, University of California, Davis, CA, 1987.